Modeling Self-Piercing Riveted Joint Failures in Automotive Crash Structures

P.K.C. Wood[1], C. A. Schley[1], M. Buckley[2], B. Walker[3], T. Dutton[4]
[1]*University of Warwick, IARC*, Central Campus, Coventry, England*
[2]*Jaguar and Land Rover, Lighthorne, Warwick, England*
[3]*Ove Arup and Partners, The Arup Campus, Solihull, England*
[4]*Dutton Simulation, Kenilworth, Warwickshire, England*
** International Automotive Research Centre*

Abstract

This paper describes a new model and method to predict Self-Piercing Riveted (SPR) joint interlock failures in aluminium sheet at crash speeds using explicit finite element simulation. SPR interlock failure is dependent on rivet direction, which is included in the model. A mesh independent approach is adopted for connection model which is capable of industrial application at the full vehicle crash analysis level. The paper provides an overview of the approach to validate connection model; typically by developing detailed physics based models of various joint configurations supported with high speed experimental data, through to model capable of industrial application. The framework to validate joint failure model for use in crash simulation tools is expected to have broader application.

Introduction

In the automotive industry the Self-Piercing Rivet (SPR) is used to join pressings to create a body-in-white assembly. Although the SPR is usually associated with the joining of aluminum pressings and castings it is also used to join different materials such as aluminum to steel. The SPR joining technique relies on creating a mechanical interlock by flaring the hardened steel rivet shank, after it pierces a second sheet in joining a two-sheet assembly. The technique is not restricted to joining a two-sheet assembly, as it may be used to join three or more sheets comprising different materials in a single operation[1].

Researchers investigating SPR failure mechanisms[1-4] had identified three failure modes; interlock, rivet head pull through and tensile or shear fracture in the sheet material (or substrate). Specimen configurations used in these research studies include peel, shear, cross-tension and u-tension angular arrangements. The dimensions of specimens used in these different research studies vary, and variations appear largely dependent on speed of test. Specimens used in low speed (quasi-static) tests tend to have a larger width dimension typically between 40 and 50 mm. Specimens used in high speed tests tend to have a smaller width typically below 30 mm. A higher joint strength normally accompanies wider specimens and especially the SPR[5].

The interlock strength of a self piercing riveted joint is determined by the frictional force between rivet shank and substrate, together with the angle at which rivet flares into second sheet[1,6]. The highest joint strength is expected where the joint interlock fails, rather than fracture in the substrate, since the later indicates the load carrying capacity of substrate is lower than rivet interlock strength.

This reported study is focused exclusively on modeling the SPR joint interlock failure mode in a two sheet assembly, using the same aluminum alloy sheet material and gauge in either substrate.

Experimental Investigations

Three specimen configurations are used to develop test data to validate models. These are lap shear, peel and u-tension configurations. The three specimen configurations are shown below as they are set-up for testing across the speed range from quasi-static to 5 m/s in a servo-hydraulic high speed test machine following the recommendations[7-8].

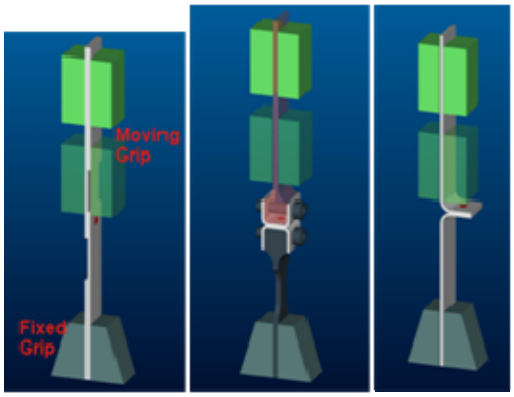

IARC joint specimens set up for high speed testing:

Lap shear (left)
U-tension (middle)
Peel (right)

The fast jaw is set to clamp specimen at the same distance[7] between fixed and moving grip for lap shear and peel specimens at all test speeds. The SPR joint is midway between fixed and moving grip at the start of specimen loading. The specimen width for high speed joint testing is fixed at 29mm for all three specimen configurations.

Manufacture of specimens: The sheet material to manufacture all joint specimens is a Novelis aluminium alloy AA5000 series at 2.5 mm gauge. The material selected is a work-hardening grade intended for structural applications in which strength increases with the amount of cold work introduced. All joint specimens were produced to Jaguar and Land Rover quality requirements by Henrob[5]. A simulated paint bake heat treatment was applied to some of the specimens for each configuration after the specimens had been joined to condition them in the same way as the body in white. An advantage for model validation studies being the thermally activated recovery process in the material reduces the level of local work hardening introduced by the rivet piercing process; this reduces variation in mechanical properties across specimen.

Test results: SPR interlock failure was observed for all specimen configurations tested and at all test speeds. Test results for lap shear, u-tension and peel specimens are shown in figures 2 to 4. In the graphs, the force in global X is the load measured by machine sensor. Grip displacement is actually the measured movement of actuator. The relative movement between actuator and grip is so small however compared to displacement of specimen they are considered the same. The same measurement descriptions are used in the analysis of models.

Figure 2a shows deformation of lap shear specimen is not symmetric, whilst figure 2b shows simulated heat treatment slightly flattens the response, reducing interlock strength, but increasing displacement to failure. The same is observed for u-tension specimens in figure 3, and the difference is more acute for the peel specimens in figure 4. The speed effect as shown in figure 4c for peel specimen result has by comparison to the heat treatment negligible effect on performance, and similarly for lap shear and u-tension specimens (graphs not provided). Finally, test results for the three specimen configurations suggest performance is predictable.

Numerical Investigations

Modeling investigations using LS-DYNA®[9] and Oasys Environment[10] proceeded at three levels by developing;

1. Detailed physics based models
2. Refined shell element models
3. Engineering scale (or substitute) model

The material was tested at both low and high speed to establish material input to substrates in models of joint specimens[11].

1. Development of physics based models

Development of u-tension physics based model: The rivet geometry of a typical u-tension specimen is measured after testing, see figure 5. These measurements together with un-deformed specimen geometry are input to physics based model shown in figure 6a. Fully integrated solid elements around 0.5 mm in length describe deformable parts of specimen. Although structurally homogeneous, the deformable half of model is described in parts e.g. sleeve, corners and central body of deformable specimen, to enable variations to be tested to support model validation. For example, to test effect of constraint on interlock strength by switching a deformable part to rigid, and similarly to test effect of mechanical property variation by parts.

U-tension physics based model validation: The model deformed geometry of figure 6b is consistent with the deformed test specimen geometry of figure 5a. Model correlation with friction coefficient set to 0.4 broadly matches the load and displacement obtained for heat treated specimen test result as shown in figure 6c. Model predicts end of loading at just over 4 $^{1}/_{3}$ mm displacement compared with 5 mm in test result. The difference is not great but note rivet side of specimen is modelled as a rigid part, and a small elastic extension in the fixture which is not modelled either, taken together amount to ½ mm in compliance deficit.

The capability of physics model is further demonstrated by introducing representative work-hardened mechanical properties in the corners and sleeve of specimen. The U-tension specimens are fabricated by folding rather than stretch-drawing, which results in plastic bending at the corners. The average absolute strain across the section in the corners resulting from bending is estimated at 4%; a higher material flow stress is introduced to corners and sleeve by offsetting the material strain axis by the same. The resulting correlation with test result for specimen which did not receive heat treatment is very good, see figure 6d.

Interlock Resistance: The model suggests rivet is being pulled out of sleeve whilst body of specimen is also being stretched from fixture, see figure 7a. Experiments confirm this observation[12], which may be described by two springs in series. One spring (k1) represents resistance of specimen. The other spring (k2) represents resistance of interlock and deformation is mostly non-reversible[6]. The force to pull rivet from sleeve - ***interlock resistance*** - increases with degree of constraint around connection or more generally resistance of specimen as shown in figure 7b, hence k2 = f(k1). Increasing interlock resistance will lead to failure in substrate. The coupling between interlock resistance and resistance of specimen suggests an ***Explicit Model*** of connection may be needed to enable full predictive model capability in industrial applications. This project is developing an ***Implicit Model*** of connection**.**

The force carried by both springs in a series spring model is always equal and the total extension is the sum of both spring extensions, which corresponds to the measured grip displacement. The interlock resistance (k2) is the input to engineering scale (or substitute) model of connector. The simplest approach to determine k2 is to scale the grip displacement axis of the measured force-displacement curve in direct proportion its relative displacement (rivet displacement in sleeve).

Lap shear physics based model: The laps shear physics model of figure 8a was developed and validated in the same way as u-tension physics model. The deformed shape of model resulting from interlock failure is consistent with test result see figure 8b and 8c. In summary;

- Stretch in diameter of sleeve due to shear loading is measurable and typically 1 ¼ times the original diameter of interlock in clamp side of specimen, see figure 8d
- Bending around rivet axis resulting from off axis shear loading is measurable at about 45^o
- Rivet pull out (interlock failure) results from shear and bending
- Interlock failure has direction dependency, having implications for engineering scale model

2. Development of refined shell element models

Main purpose of refined shell element models is to validate measurements, establish contact thickness scale setting for connection, and support validation of engineering levels models.

Measurements include force and displacement and in testing they are measured remote from point of interest (connection). In testing, it is necessary to establish relationship between measured force and force at connection. Further, in dynamic testing a remote sensor results in a delayed signal response and increasing measured load oscillation due to compliance and mass of load train elements. Delayed response is not normally a problem for servo-hydraulic systems because speeds operate below 20m/s, and measurement locations are not too distant from the point of interest. At the expense of increased complexity and cost measurements may be positioned more closely to position of interest. The refined shell element model of each joint configuration will determine where measurement locations should be sited for practical dynamic joint testing up to 5m/s, and the relationship to measurement at connection.

Fully integrated quadrilateral shell elements of 1mm length are used in refined shell models of each joint configuration. The connection is modeled using a stiff multi-hex cluster of solids with elastic property definition. Figure 9a shows model construction details of u-tension test.

Refined u-tension shell element model: Force measurement locations from u-tension test with grip speed set to 5 m/s are compared in figure 9b. The frequency response of local force transducer on static fixture is improved on the machine force sensor measurement; both measurements are consistent with contact force measurement local to connection. However the initial rise in load signal from machine sensor does not capture the local event at connector. The local force transducer on fixture delivers a wave length 2 x machine based sensor. This is sufficient to give around 5 to 6 full oscillations over 4 mm displacement, to discern speed effect on performance, compared with 3 from machine based sensor.

Refined peel shell element model: The peel specimen and test configuration is more compliant than u-tension specimen as the grip extends to near 20 mm extension before joint fails. Hence machine force sensor enables measurement at 5 m/s over the entire event see figure10a. The local force sensor (strain gauge) on specimen is unreliable. The contact force measurement local

to connection is around 30% higher than machine force sensor measurement. Analysis of forces on peel specimen at connection is shown in figure 10b. The local reaction forces R1 and R2 can not be measured directly from test. Neither can they be determined from equilibrium, they are statically indeterminate. The peel model confirms force balance.

Refined lap shear shell element model: Force measurement locations from lap shear model with grip speed set to 5 m/s are compared in figure 11a. The frequency response of local force transducer on specimen is improved on the machine force sensor measurement, and both measurements are consistent with contact force measurement local to connection. The lap shear joint fails at slightly higher grip displacement than u-tension specimen. This is sufficient to give around 5 to 6 full oscillations from machine force sensor over 6 mm displacement, to discern speed effect on performance.

The connection rotates as load is introduced to lap shear specimen, see figure 11b. Machine force sensor measurement (Fx Global Axis) is always in the global axis reference. Component reaction forces at connection in relation to local axis reference are determined by the change in angle of connection[2-3], which is very nearly linear with grip displacement[6], to convert test measurements from global axis reference as follows;

$$Fx\ (\text{local axis}) = \{Fx\ (\text{global axis}) \times \text{Cosine}(\theta)\} + \{Fz\ (\text{global axis}) \times \text{Sine}(\theta)\}$$

$$Fz\ (\text{local axis}) = \{Fx\ (\text{global axis}) \times \text{Sine}(\theta)\} - \{Fz\ (\text{global axis}) \times \text{Cosine}(\theta)\}$$

Fz (global axis) is zero for lap shear joint configuration and confirmed by model which simplifies the equations by eliminating the second term in brackets.

3. Development of engineering scale (or substitute) model

This is the scale used in engineering design in virtual testing of engineering crash structures. The approach will use a fully integrated shell element and size approaching the engineering scale (approx 6 mm side length) to model substrates for all joint specimen configurations. A 6dof non-linear discrete plastic beam will model connection and validate inputs; discrete beam is attractive because direction property inputs are uncoupled and interlock offers virtually no twist resistance. Variations will include testing boundary conditions of connection e.g. released rotations at one and both ends, and directional property inputs. A mesh independent approach will be adopted to test variations.

U-tension substitute model validation: Model of u-tension joint specimen configuration is shown in figure 12a. Tension interlock resistance (k2) input to discrete beam is shown in figure 12b, and is determined by scaling grip displacement axis. The hashed line in figure 12b is k2, and is set constant on reaching maximum load until failure. Loading of discrete beam element is unidirectional in u-tension test so boundary conditions e.g. released rotations at beam ends, has no effect, and neither does transverse shear and flexure property inputs. Displacement based failure is introduced to connection in tension axis by inputting 3.7 mm (figure 5c) to discrete beam material definition. Force measurement from u-tension physics model and substitute model are in excellent agreement to maximum load, see figure 12c.

Lap shear substitute model validation: Model of lap shear specimen configuration is shown in figure 13a. Effect of boundary condition inputs to discrete beam e.g. released rotations at beam ends, is tested by constraining plastic deformation and displacement based failure to local tension axis of beam. Physically, rivet interlock failure will always develop in the local tension axis. There will however be a small, but measurable plastic deformation in the local shear axis as shown in the lap shear physics model by elongation of sleeve. Constraining plasticity to the local tension axis of beam is expected to give an over stiff result. The elastic stiffness inputs to beam are determined for 5 dof (3 translation, 2 rotation, twist along principal beam axis is released). Figure 13b compares the effect of beam end release conditions with plasticity and failure constrained to local tension axis of beam on force measurement. Rotations released at one end of beam which correspond to interlock failure, gives the best model fit to test results; although over stiff which was expected. Also the non-symmetric mode of deformation for beam with rotations released at one end is consistent with test results and physics model, see figure 13c.

Shear interlock resistance: To test model with shear plasticity introduced to beam and rotations released at one end, it is first necessary to determine the shear component reaction force at connection in relation to local rivet axis reference, see figure 13d. The beam local axis reference enables a decoupling of tension and shear plasticity. Shear plasticity or shear interlock resistance (s2) input to beam is shown in figure 13e and determined by the method of scaling grip displacement axis. The material card for discrete beam now contains separate inputs for tension and shear interlock resistances. Displacement based failure is constrained to local tension axis as before. An improvement in model fit to test result is shown in figure 13f.

Peel substitute model validation: Model of peel specimen configuration is shown in figure 14a. Using the same material card for discrete beam as used in lap shear substitute model with tension and shear interlock resistance inputs, and displacement based failure constrained to local tension axis, machine force sensor measurements are compared for different beam end restraints in figure 14b. Rotations released at one end shows the best fit to test result. Similarly mode of deformation with rotations released at one end is consistent with test results, see figure 14c.

Although the peel test does not provide direct physical data input to model of connection, it does enable a check on numerical input which effect physical measurements. Local reaction forces R1 and R2 in peel substitute model must be consistent with refined shell element model. Local reaction forces in the peel substitute model were found to be sensitive to some control settings, which could be made stable and accurate, whilst machine force measurement F1 remained largely unaffected. Therefore peel test is a necessary validation test at the specimen level.

Summary of inputs to substitute connection model

Model requires 3 inputs to describe non-reversible deformation;

- Tension interlock resistance (k2) and local rivet displacement to failure, both derived from u-tension test
- Shear interlock resistance (s2) derived from lap shear test

Model requires 5 inputs to describe reversible deformation;

- 3 elastic translations (1 axial and 2 shear) and 2 elastic rotations (twist released), which may be derived from the same u-tension and lap shear joint tests used to generate the 3 non-reversible inputs

Concluding Summary

- Test results from the three joint configurations lap shear, peel and u-tension suggest performance is predictable, and interlock failure is observed in all specimens tested at all speeds
- The speed effect has by comparison to heat treatment negligible effect on performance in the speed range tested
- Self pierced rivet interlock failure is dependent on direction of rivet in substrate, and connection model with rotations released at one end gives best qualitative and quantitative correlation to test results
- A mesh independent approach was adopted using a 6dof non-linear discrete plastic beam to enable direction failure of connection model, and technique to have industry scale application potential
- Local reaction force at connection in peel joint configuration is statically indeterminate, and although it doesn't provide direct physical input to connection model it is a necessary validation test at the specimen level
- The framework to validate the joint failure model at specimen level for use in full vehicle crash simulation is expected to have application to other joining methods

Forward: Validate joint failure model at full vehicle application scale. Enhance capability of joint failure model to include rivet head pull through and material-substrate failure.

The content of this paper is believed to be substantially original except where referenced.

References

1. L. Han, A. Chrysanthou, K.W. Young, Mechanical behaviour of self-piercing riveted multi-layered joints under different specimen configurations, Materials & Design 28 (2007), p2024-2033, Elsevier.
2. R. Porcaro, A.G. Hanssen, A. Aalberg, M. Langseth, Joining of aluminium using self-piercing riveting: Testing, modelling and analysis, IJCrash 2004, vol 9, No.2, pp141-154, Woodhead publishing Ltd.
3. R. Porcaro, A.G. Hanssen, M Langseth, A. Aalberg, An experimental investigation on the behaviour of self-piercing riveted connections in aluminium alloy AA6060, IJCrash 2006, Vol 11, pp379-417, Woodhead publishing Ltd.
4. C. Madasamy, O. Faruque, T. Tyan, R. Thomas, Static and dynamic behavior of self-pierced rivet connections in aluminium, Proc ASME International Mechanical Engineering Congress and Exposition, Nov 2001, NY, USA
5. H. Litherland, Self-Piercing Riveting - Effect of coupon geometry of static shear strength, May 1999, Henrob report ref: DP1424 issue 2, Henrob UK.
6. 11th Crash Guild meeting, hosted by University of Warwick, reported January 2008.
7. P.K.C. Wood, C. A. Schley, et. al. Recommendations for dynamic testing of joints in sheet metals and alloys for automotive crash applications, Premium automotive research and development, March 2008 (1st draft document), IARC, University of Warwick.
8. VDEh working group meeting to develop industry standards for high speed testing of welded steel joints, 3rd meeting October 2007, German Stahl Institute, Dusseldorf, Germany.
9. Hallquist, J. O., LS-DYNA. Keyword User's Manual. Version 971, Livermore Software Technology Corporation, Livermore, 2007.
10. OASYS LS-DYNA ENVIRONMENT, The Arup Campus, Blythe Valley Park, Solihull, West Midlands, B90 8AE
11. P.K.C. Wood, C. A. Schley, et. al. Recommendations for dynamic testing of metallic materials and their modelling for use in CAE based automotive crash simulation tools, Premium automotive research and development, February 2008 (2nd draft document), IARC, University of Warwick.
12. M. Buckley, X351 / PLA U Tension SPR cross sectional samples, report no. 6405552, Jaguar and Land Rover Materials Engineering Laboratory Report, February 2008.

Acknowledgements: Crash Guild members and project partners include ARUP, ARRK, Corus, Dutton Simulation, GOM UK, HBM, Henrob UK, Jaguar and Land Rover, MIRA, Novelis UK, Ricardo and grant provider for 12 month project Advantage West Midlands in UK.

Contact: Dr Paul Wood, Principal Author, Lead Engineer and Project Manager in Crash Materials Technology within the Premium Automotive Research and Development Programme at the IARC. Email: P.K.C.Wood@warwick.ac.uk / UK (0) 7932 608084

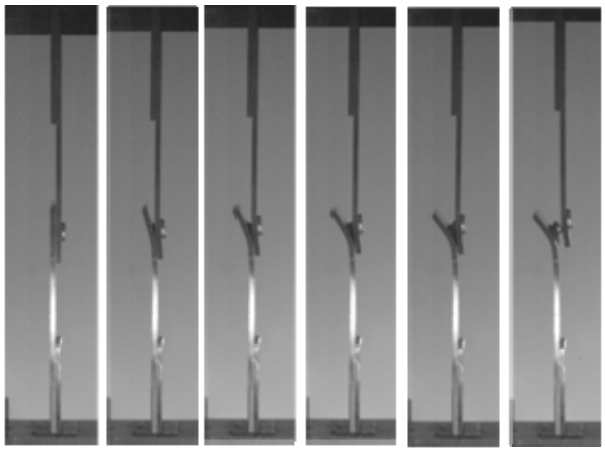

Figure 2a: Lap shear - digital camera recording of heat treated specimen tested at low speed

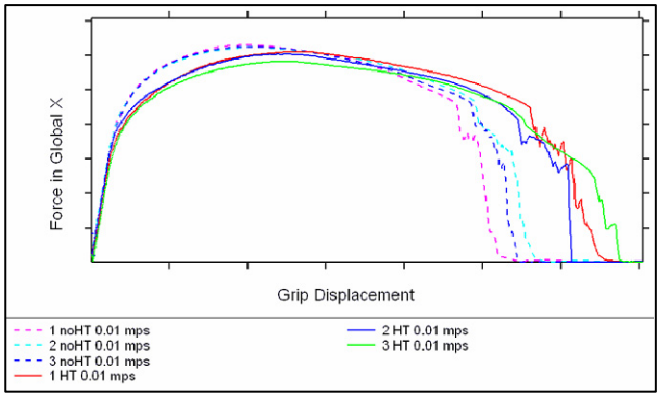

Figure 2b: Lap shear - solid curve specimens received heat treatment, hashed curve specimens did not

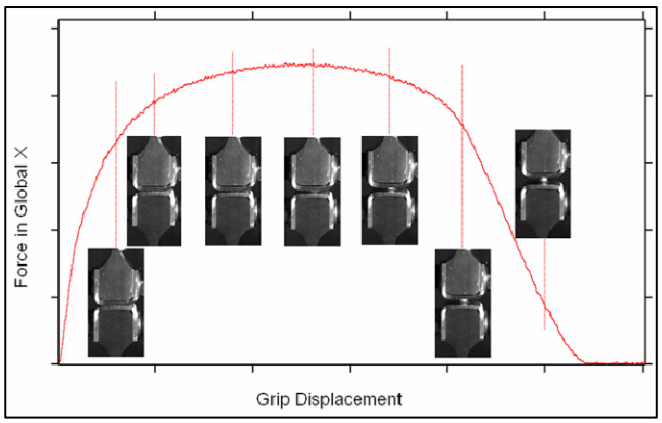

Figure 3a: U-tension specimen - digital camera recording synchronised to low speed test result for heat treated specimen

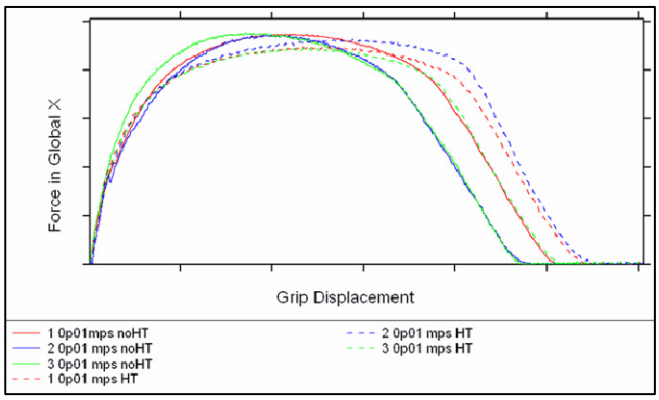

Figure 3b: U-tension specimen - hashed curve specimens received heat treatment, solid curve specimens did not

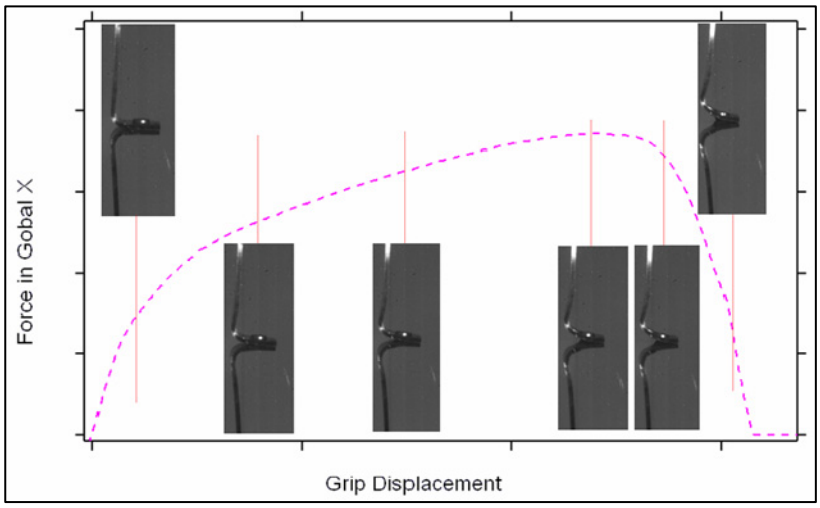

Figure 4a: Peel specimen - digital camera recording synchronised to low speed test result for heat

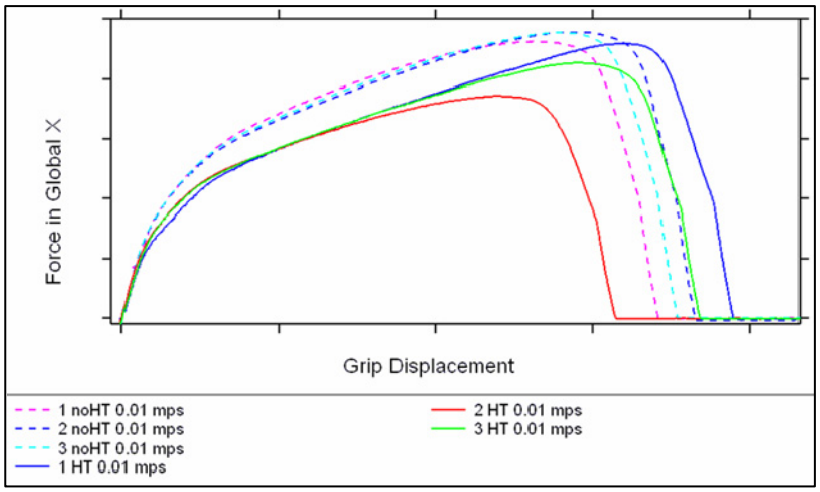

Figure 4b: Peel specimen - solid curve specimens received heat treatment, hashed curve specimens did not

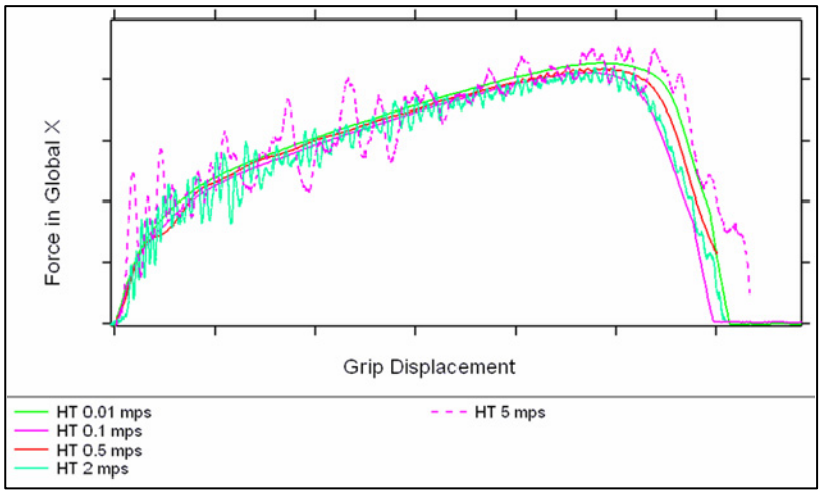

Figure 4c: Peel specimen - effect of test speed on peel specimens which received heat

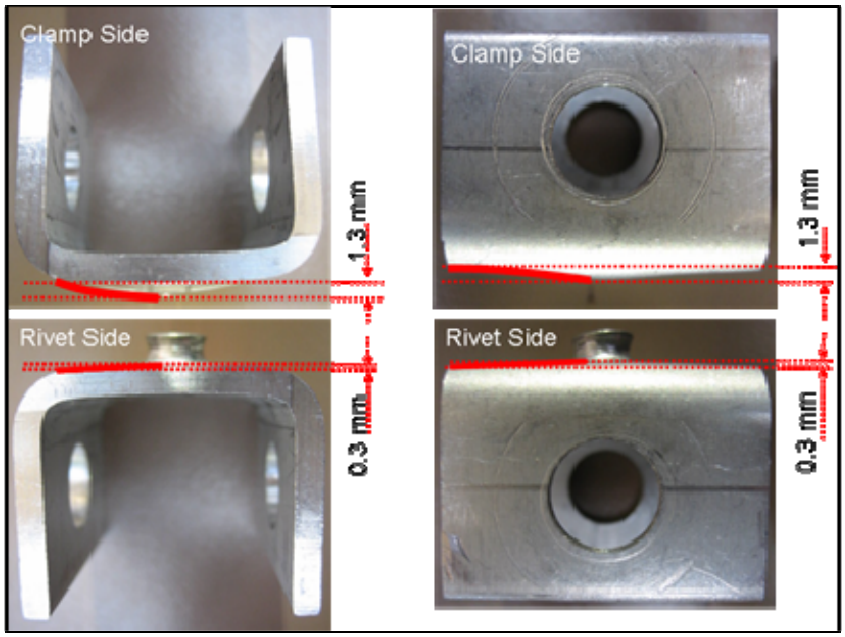

Figure 5a: Geometry of u-tension specimen measured after testing

Note: Deformation of specimen clamp side is much greater than rivet side

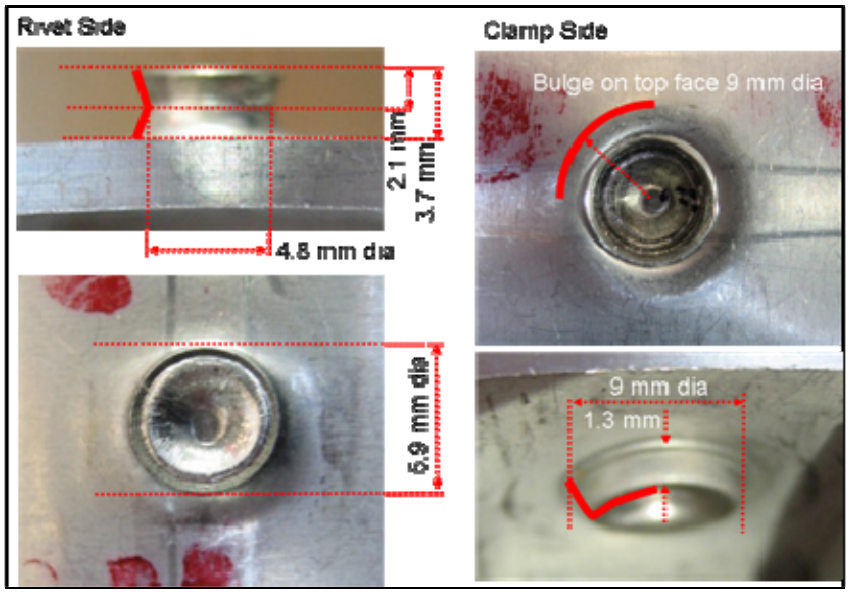

Figure 5b: Rivet geometry of u-tension specimen measured after testing

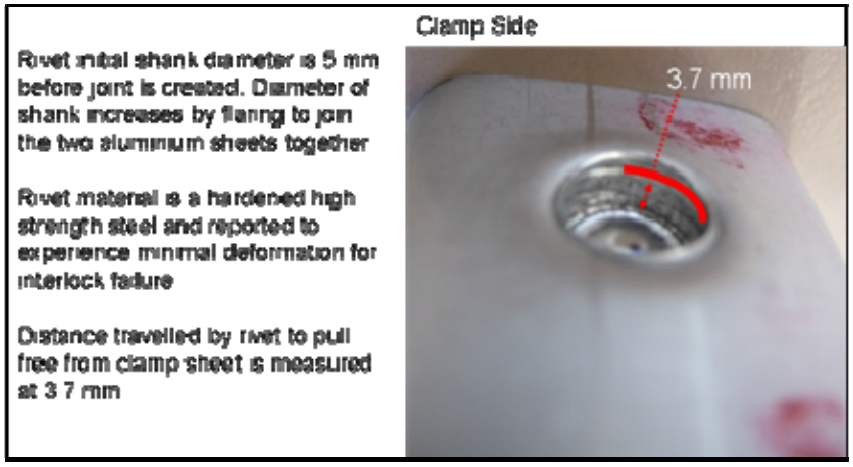

Figure 5c: Rivet material hardened steel (assumed not to deform)

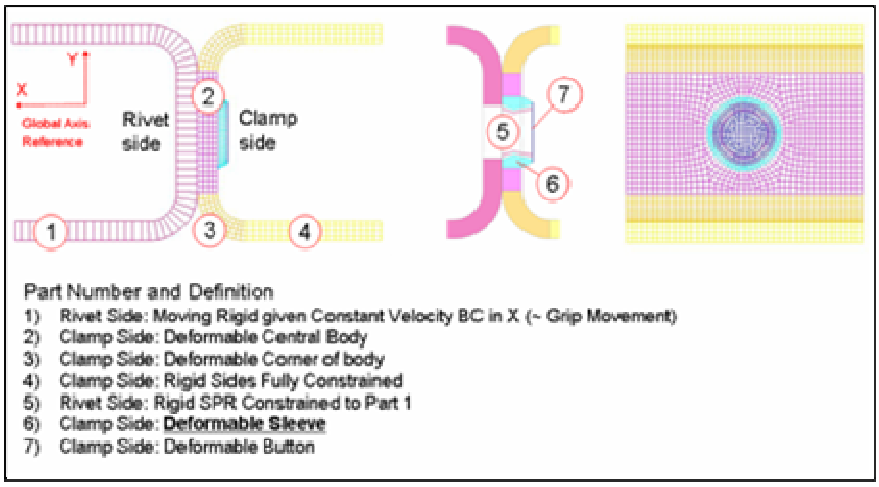

Figure 6a: Development of u-tension physics based model

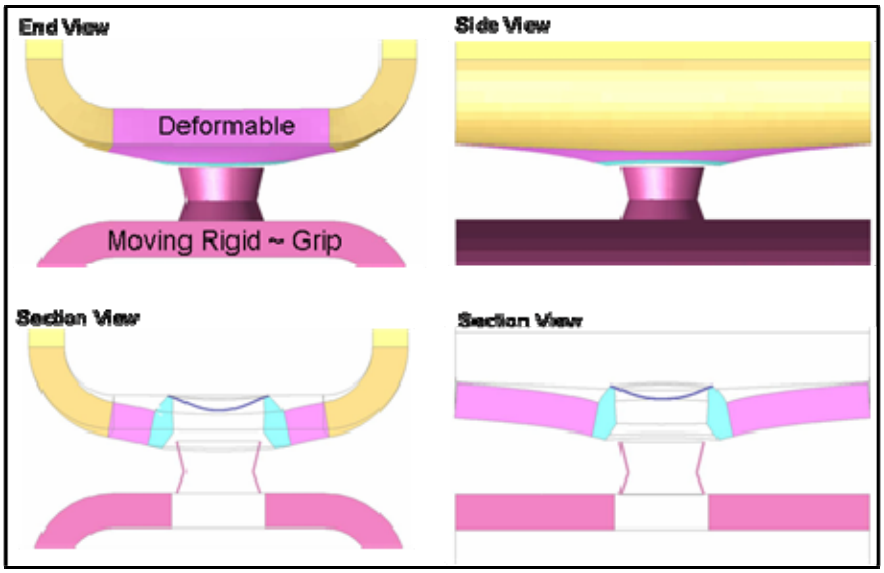

Figure 6b: U-tension model deformed shape

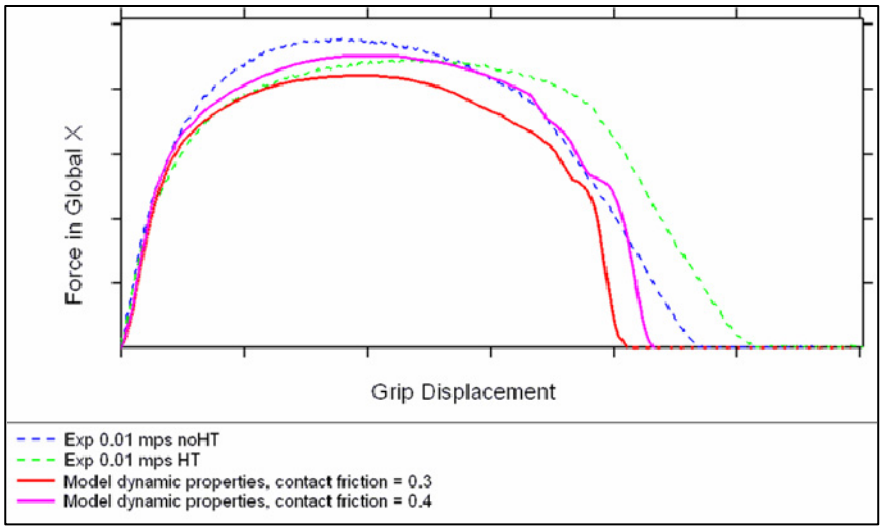

Figure 6c: Effect of friction - compare contact force from model with test result (HT = heat treatment)

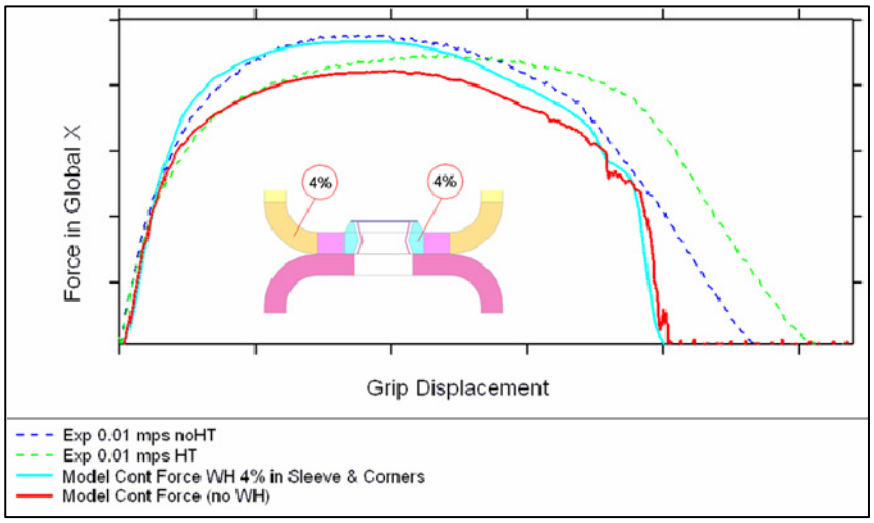

Figure 6d: Effect of work-hardening - compare contact force from model with test result (HT = heat treatment)

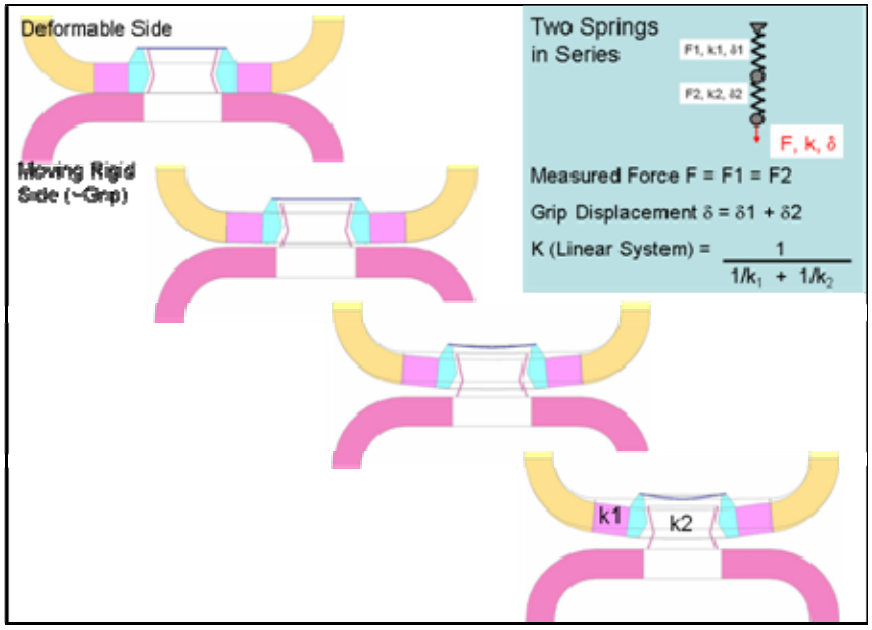

Figure 7a: U-tension model may be represented by series spring with 2dof

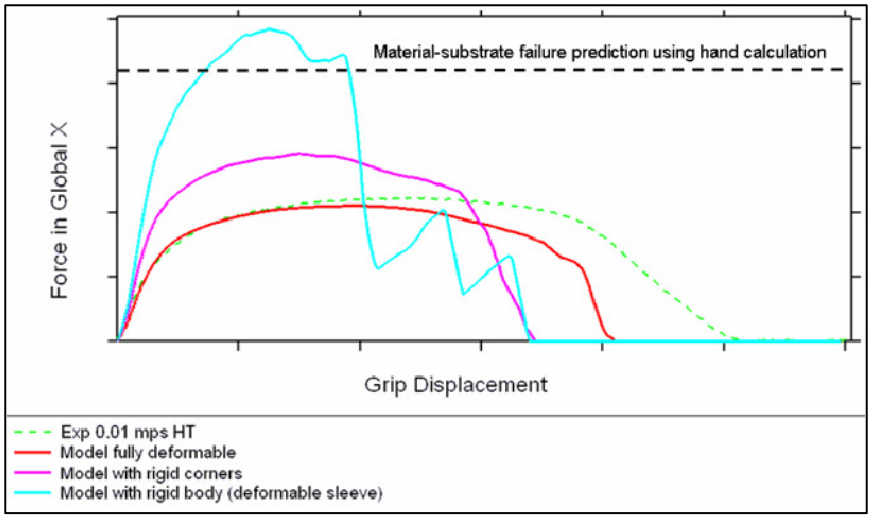

Figure 7b: Effect of constraint on interlock - compare contact force from model with test result (HT = heat treatment)

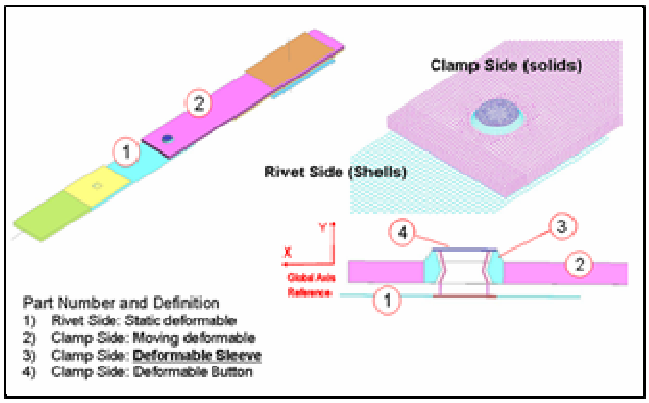

Figure 8a: Development of lap shear physics model

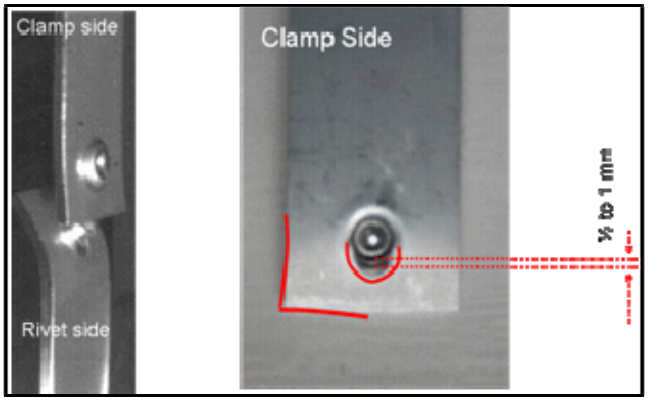

Figure 8b: Post test measurements of deformed specimen

Note in plane stretch of clamp side and bending of rivet side

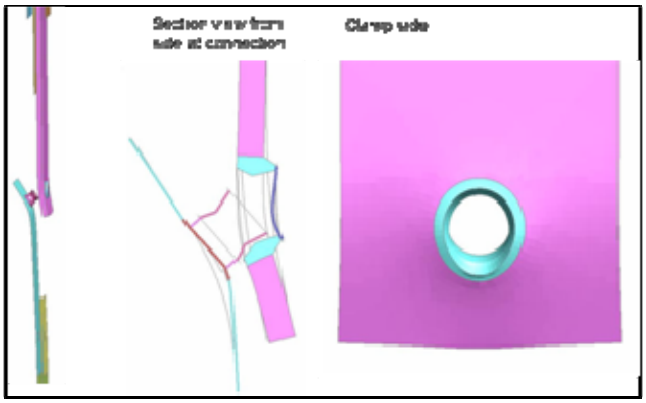

Figure 8c: Deformed shape of lap shear SPR model

Deformed shape corresponds to test specimen geometry

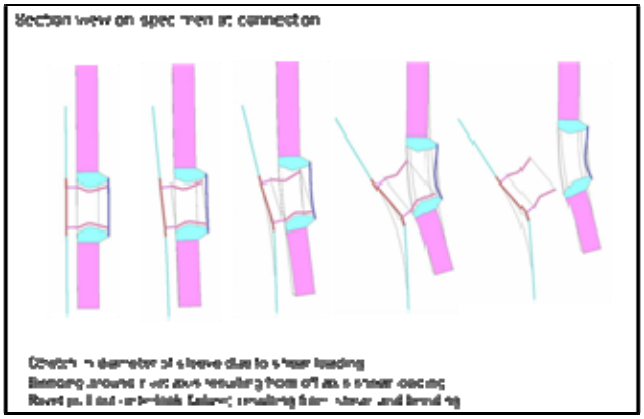

Figure 8d: Deformed shape of lap shear SPR model

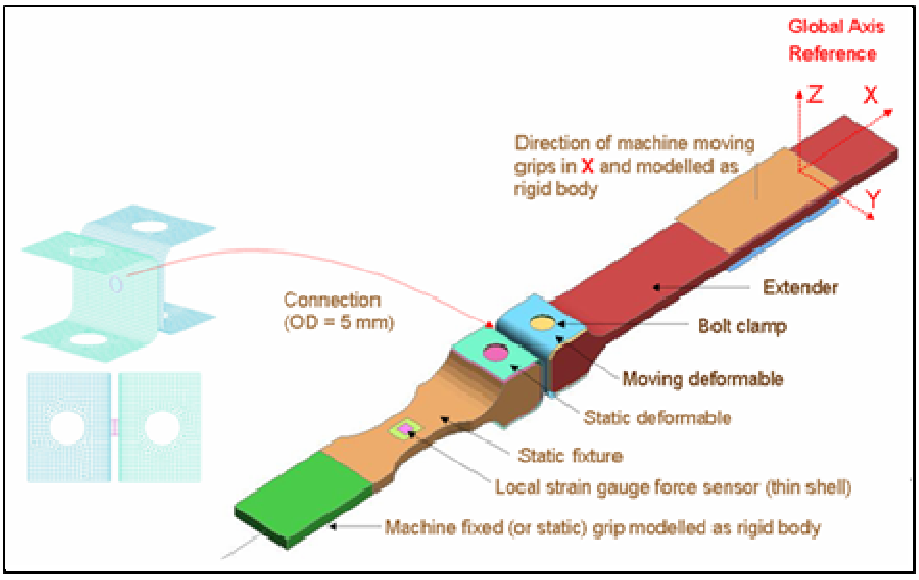

Figure 9a: U-tension model using detailed shell elements and stiff connection

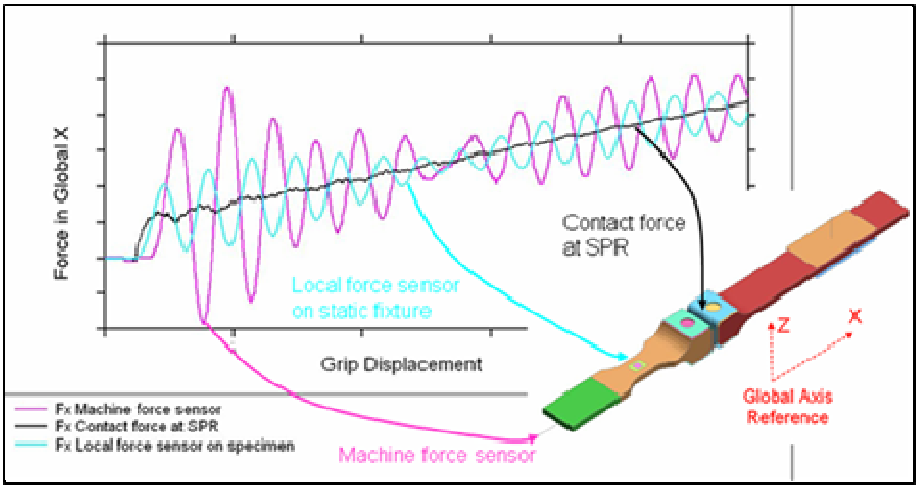

Figure 9b: Comparing force measurement locations from u-tension model in global axis reference

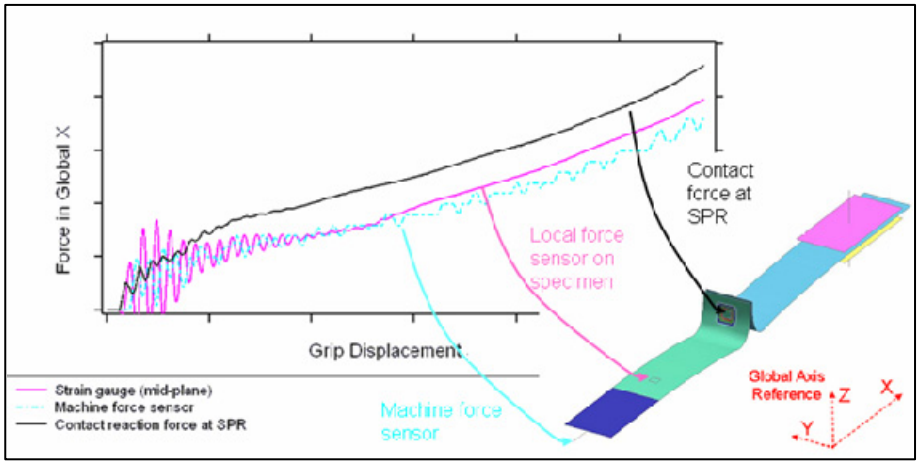

Figure 10a: Comparing force measurement locations from peel model in global axis reference

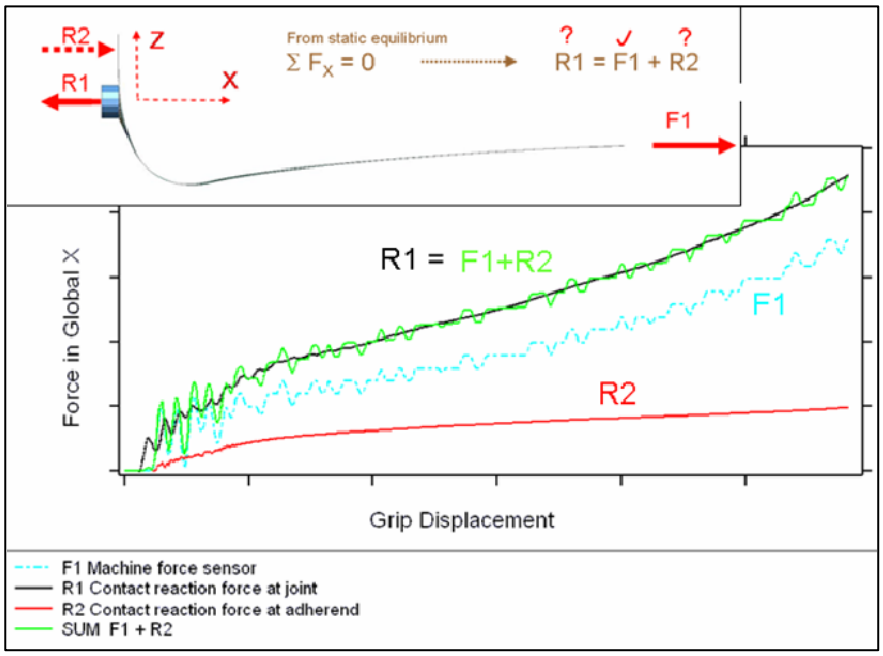

Figure 10b: Confirming static equilibrium in peel model in global axis reference

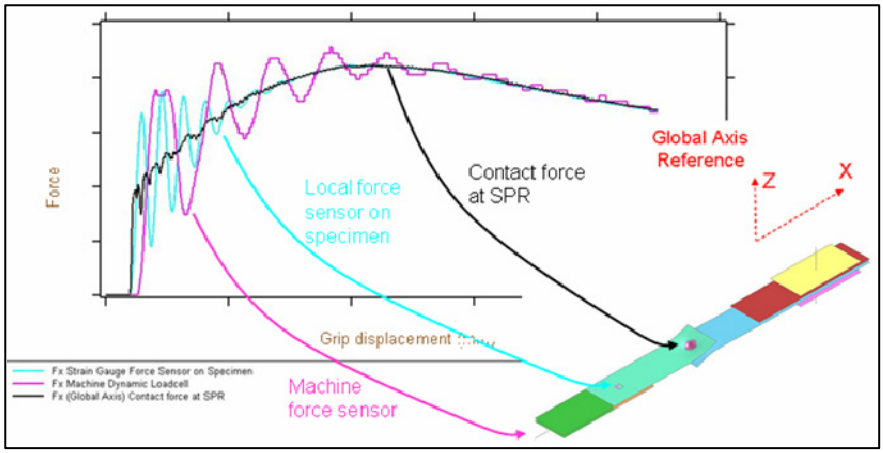

Figure 11a: Comparing force measurement locations from lap shear model in global axis reference

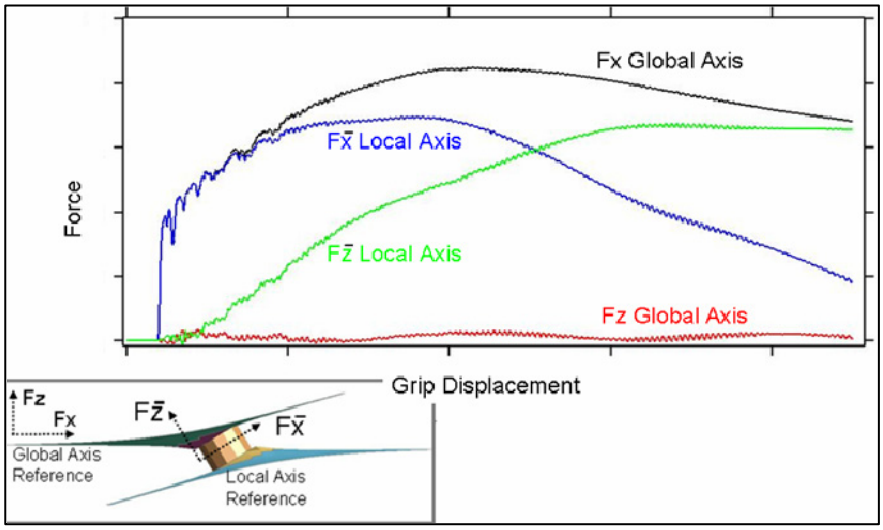

Figure 11b: Comparing measurements in global and local axis reference systems at connection

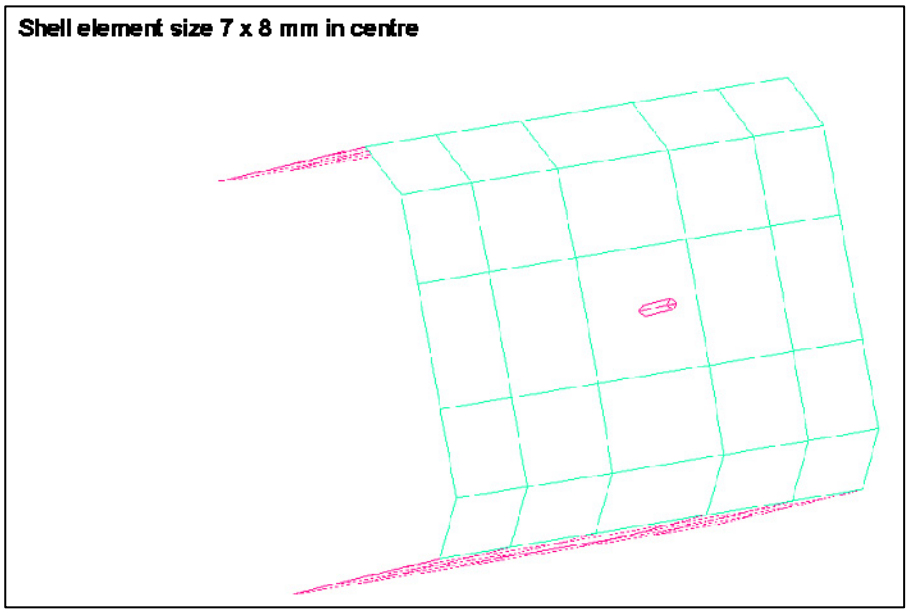

Figure 12a: U-tension engineering scale model and connection modelled with discrete beam

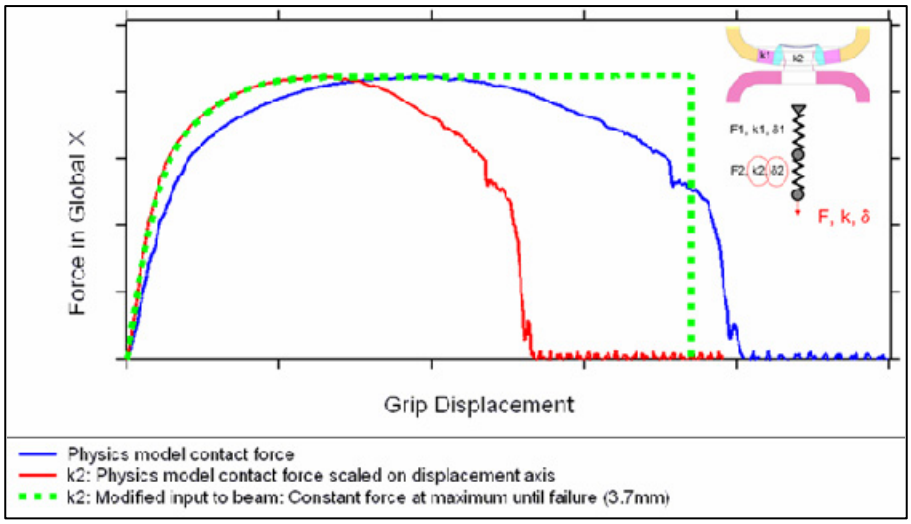

Figure 12b: Tension interlock resistance (k2) together with displacement based failure input to discrete beam

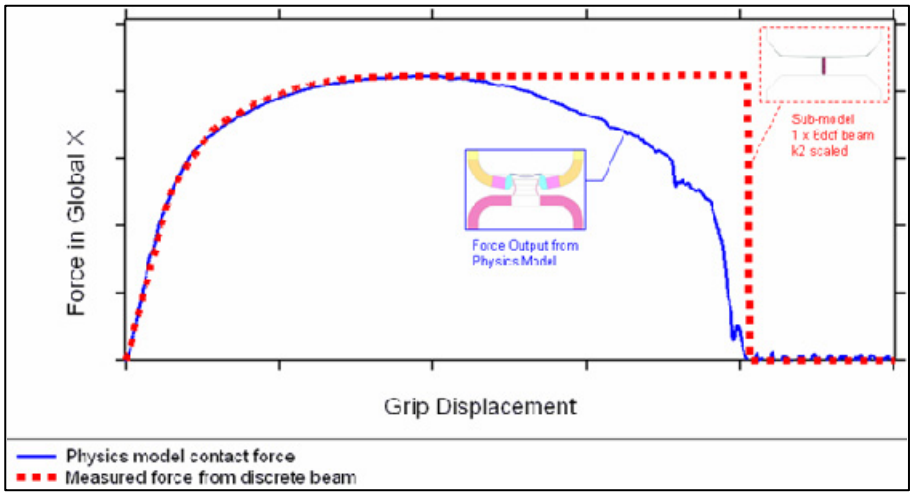

Figure 12c: Comparing force measurement in u-tension

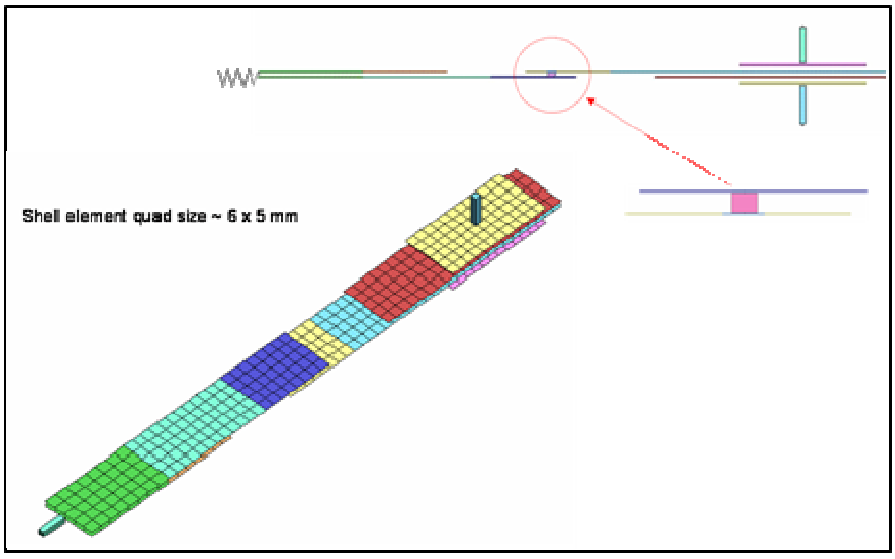

Figure 13a: Lap shear engineering scale model, connection modelled with discrete beam

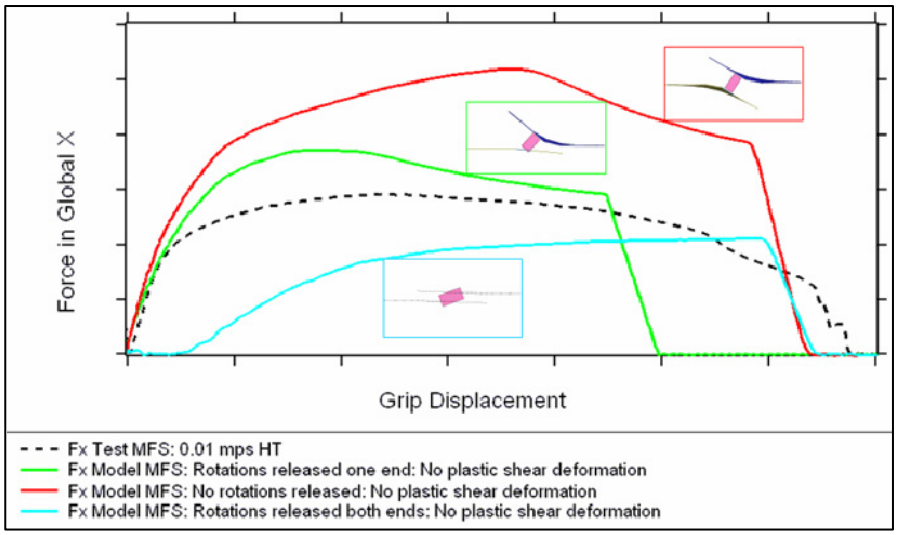

Figure 13b: Comparing measurements from machine force sensor (MFS) for different beam end release conditions

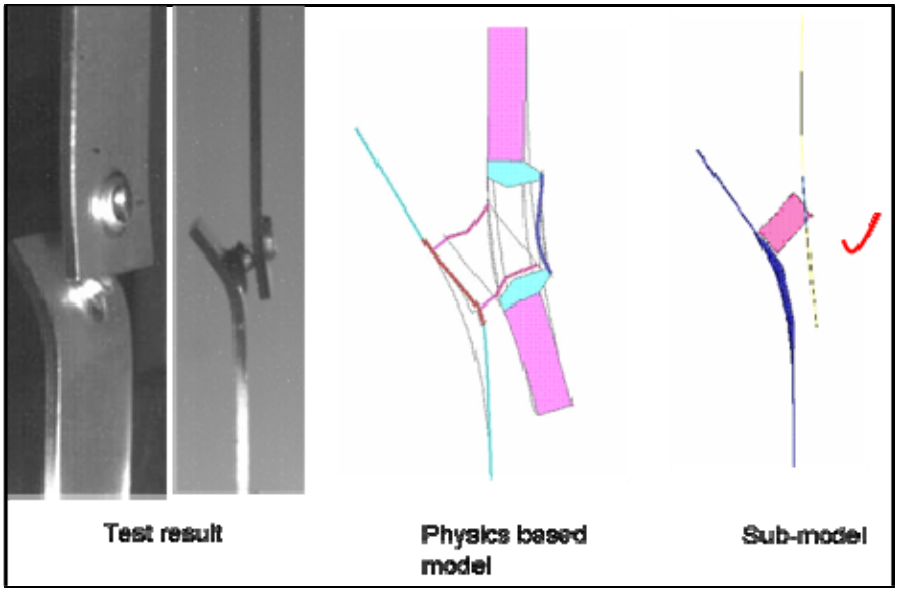

Figure 13c: Lap shear engineering scale model non-symmetric mode of deformation (all rotations released at one end) corresponds to test results and physics model

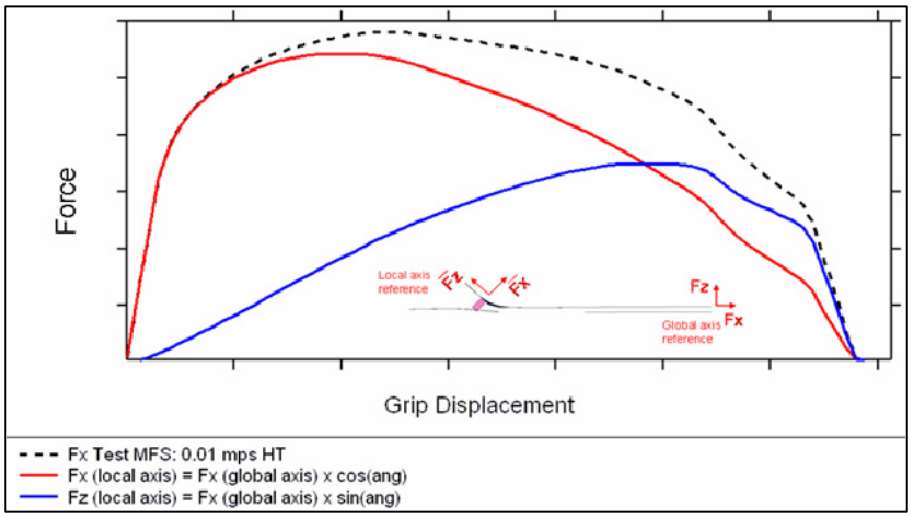

Figure 13d: Component reaction forces at connection determined in local rivet axis by converting test result (machine force in global axis reference)

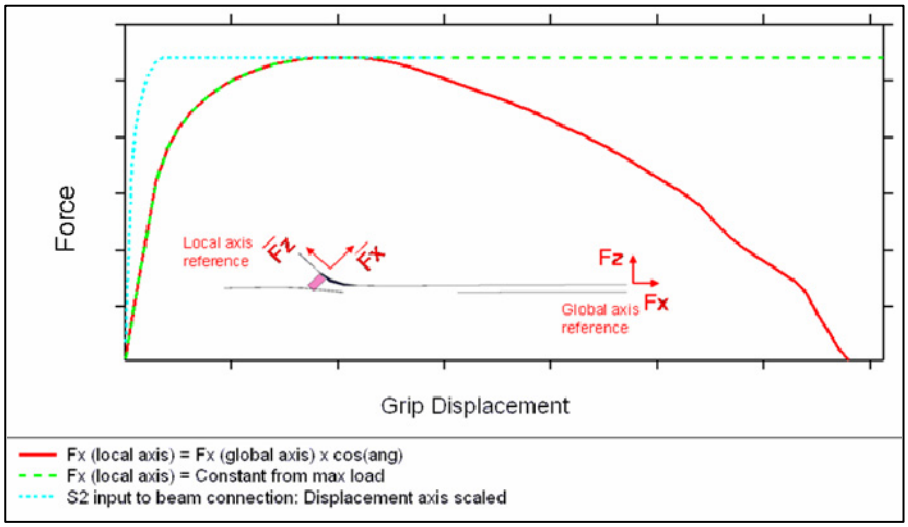

Figure 13e: Establish shear plasticity or (shear interlock resistance s2) for beam input

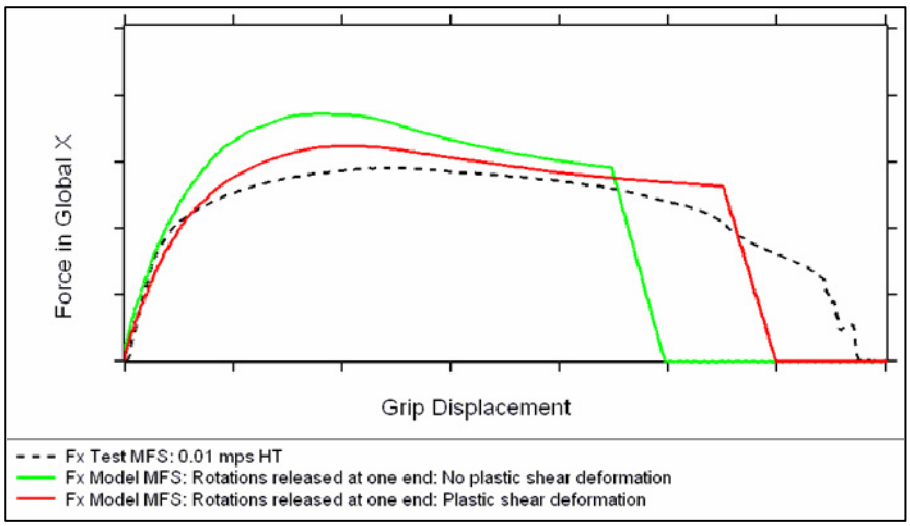

Figure 13f: Effect of introducing shear and tension plasticity to beam on force measurement

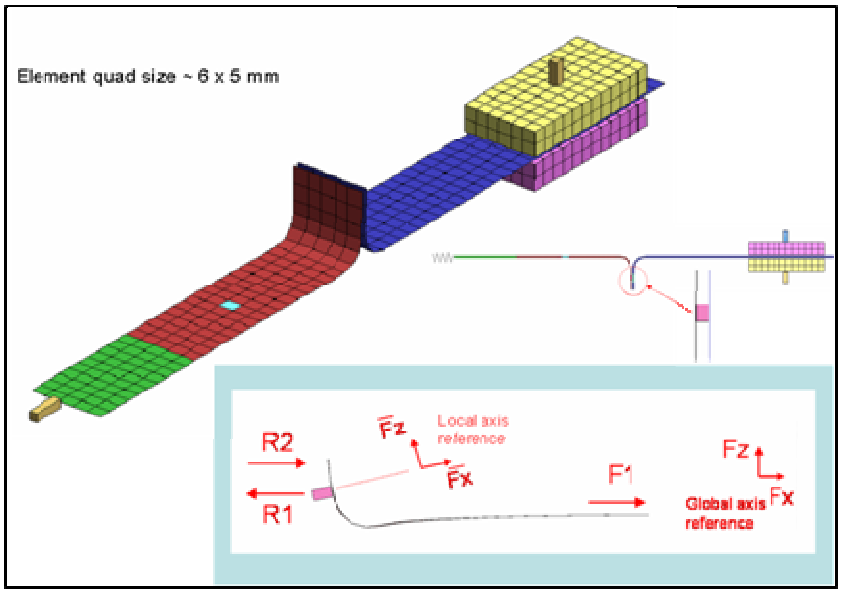

Figure 14a: Peel engineering scale model, connection modelled with discrete beam

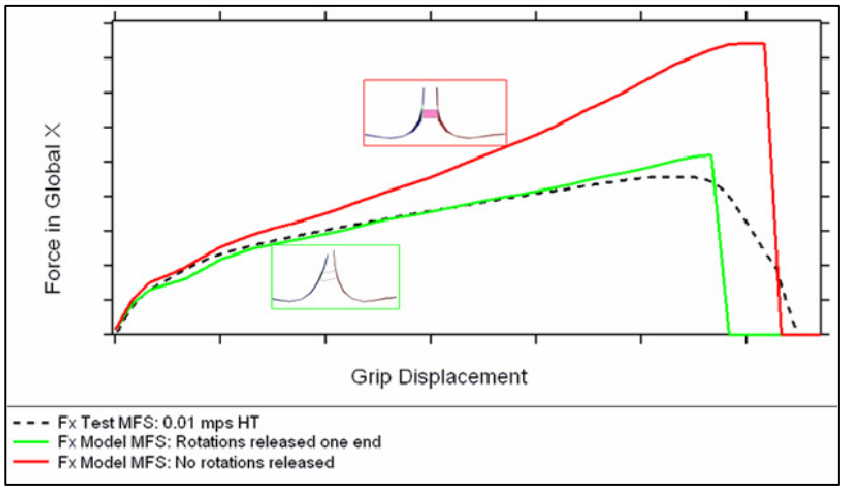

Figure 14b: Comparing measurements from machine force sensor (MFS) for different beam end release conditions

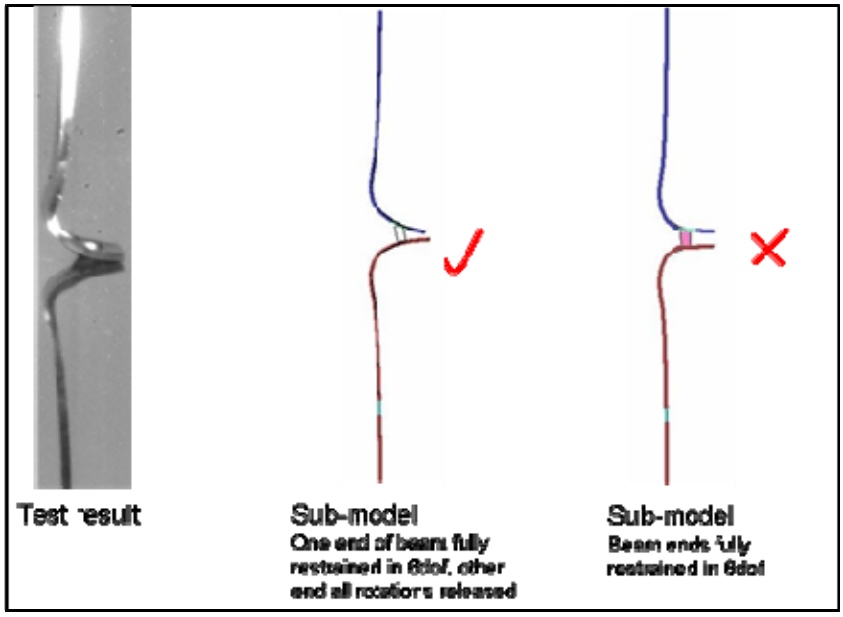

Figure 14c: Peel engineering scale model mode of deformation (all rotations released at one end) corresponds to test results